From disordered quantum walk to physics of off-diagonal disorder

Qifang Zhao and Jiangbin Gong
Department of Physics, National University of Singapore, Singapore 117546, Republic of Singapore
(Received 24 May 2015; published 31 December 2015)

Systems with purely off-diagonal disorder may have peculiar features such as the localization-delocalization transition and long-range correlations in their wave functions. To motivate possible experimental studies of the physics of off-diagonal disorder (e.g., in systems with random nearest-neighbor hopping), we study in detail disordered discrete-time quantum walk in a finite chain. Starting from a transfer matrix approach, we show, both theoretically and computationally, that the dynamics of the quantum walk with disorder manifests all the main features of systems with off-diagonal disorder. We also propose how to prepare a remarkable delocalized zero mode from a localized and easy-to-prepare initial zero mode using an adiabatic protocol that changes the disorder strength slowly. Numerical experiments are also performed with encouraging results.

DOI: 10.1103/PhysRevB.92.214205 PACS number(s): 05.40.Fb, 71.55.Jv, 03.75.−b

I. INTRODUCTION

Quantum walk (QW) has been a subject of great theoretical and experimental interests. Among many QW protocols, discrete-time QW is the simplest [1], where it can be seen clearly how QW can differ strongly from classical random walk due to quantum interference effects. For example, an initially localized state in QW will spread ballistically, which is much faster than classical random walk whose mean square displacement is proportional to time. Due to this feature, one potential application of QW models is towards a fast search algorithm [2] in quantum computation [3]. It is also useful as a quantum simulator [4]. As an example of a very recent direction, QW is shown to be useful in understanding topological phases of matter in periodically driven systems [5,6].

On the experimental side, two early QW experiments in 2005 used either linear optical elements [7] or nuclear-magnetic resonance systems [8]. Since 2007, a variety of physical systems have been exploited to realize QW, including trapped ions [9,10], trapped atoms in a spin-dependent optical lattice [11], photons in an optical waveguide array [12–15], and photonic walks with interferometers [16–18]. Very recently, a photonic quantum walk without interferometers was realized [19], in which photons walk in the orbital angular momentum space.

The topic of this work is on QW in the presence of some disorder. Previously, it was numerically found that some behavior of disordered QW seems to reflect the physics of off-diagonal disorder (ODD) [20] in condensed-matter physics. The so-called ODD was first noticed in studies of one-dimensional (1D) tight-binding models (TBMs) with nearest-neighbor random hopping potential and constant on-site potential [21,22]. Compared with the more familiar disorder model where the on-site potential (diagonal term in the lattice-site representation) is random but the nearest-neighbor hopping is constant, ODD leads to peculiar physics, such as delocalization at zero energy, power-law wave-function correlation, and so on [21–30]. Specifically, the localization length $\ell(\omega)$ in 1D TBM with pure ODD is related to energy ω via

$$\ell(\omega) \propto |\ln \omega|. \tag{1}$$

As the energy ω approaches 0, the localization length ℓ diverges, indicating a delocalization transition at $\omega = 0$. At the same time, singularity in the density of states (DOS) emerges at $\omega = 0$, with the explicit DOS expression given by

$$\rho(\omega) \propto |\omega \ln^3 \omega|^{-1}. \tag{2}$$

Furthermore, the delocalized eigenstate has an unusual long-range correlation. It is shown that its ensemble averaged two-point correlation decays polynomially with the exponent $-3/2$ under the condition of strong disorder and large two-point separation [27,28,31]. It was pointed out earlier that this is a manifestation of the actual stretched exponential-decay profile of the wave function [32–35], i.e., $\psi(x) \propto \exp(-\widetilde{\gamma}|x - x_0|^{1/2})$, where $\widetilde{\gamma}$ is a constant. One may naively say that a wave function like this is quite localized. However, its Lyapunov exponent is apparently zero (which indicates that the state is delocalized [32]) because there is no exponential localization behavior.

As we have learned from decades of studies, quite a few theoretical models with disorder can be used to manifest and digest the physics of ODD. Such models include a special disordered linear chain of harmonic oscillators investigated by Dyson [23,36,37], a 1D Dirac model with random mass and some types of disordered 1D spin chains [27,28,31], 2D Dirac fermions subject to a random vector potential [38], a 1D random hopping model consisting of several parallel bipartite sublattices [39], systems with correlated off-diagonal disorder [40,41] or random long-range hopping [42], and graphene with ODD [43]. In contrast to these theoretical developments, experimental progresses on the physics of ODD have been rather limited. Doped $CuGeO_3$ is effectively a disordered spin-Peierls system possessing ODD [44–49]. Phenomena such as phase transitions and long-range orderings were believed to be related to the physics of ODD. However, direct observation of physical properties like the correlation exponent $-3/2$ was not possible in such a system. Other than spin-chain realizations, few experiments concerning ODD were reported. We note a possible experimental approach based on cold atoms under the so-called tripod scheme [29,30], but the actual experiment has not been done. Only very recently, Keil *et al.* demonstrated that a chain of optical waveguides could be used to realize an effective 1D Dirac model with

random mass [50]. In particular, with coupled series of optical chains, the authors of Ref. [50] observed the long-range correlation (in a certain range) characterized by the correlation exponent $-3/2$.

To motivate more possible experimental studies of ODD models and to demonstrate one more promising application of QW, we consider in this work a discrete-time QW in a finite chain (for simplicity we refer to it as "QW" throughout the paper) and reveal theoretically how this problem is closely connected with the issue of ODD. Our work is inspired by an early numerical study by Obuse and Kawakami [20], which showed clear signatures of the physics of ODD in disordered QW. Specifically, we first analytically demonstrate the explicit connection between a TBM with ODD and disordered QW. In so doing we focus on a specific delocalization transition energy, the zero quasienergy, which was also considered in Ref. [20]. We then show how some simple adiabatic protocols, starting from an exponentially localized 0 mode (i.e., the 0 quasienergy eigenstate), can be converted to a peculiar 0 mode possessing the physics of ODD, with satisfactory fidelity and relatively short duration of the protocol. As such, we may make use of some existing QW experimental setups to observe the unique physics of ODD. Indeed, our numerical experiments indicate that the results agree with theoretical predictions very well, including the $-3/2$ correlation exponent.

This paper is organized as follows. In Sec. II, we will introduce a model of disordered QW in a finite chain. Analysis of the model is based on the transfer matrix formalism. Sections III is devoted to some formal connections between our QW model and a TBM with ODD. In Sec. IV we shall focus on the preparation of special states that best manifest the peculiarities of ODD. The associated results from our numerical experiments will be also presented and discussed. Section V concludes this work.

II. DISORDERED QW IN A FINITE CHAIN

The standard discrete-time QW is defined via a single particle with two internal degrees of freedom. For convenience, we refer to its internal states as "spin-up" and "spin-down." The QW protocol consists of two operations, a rotation of spin through operator R, followed by a shift operation by S. Without loss of generality, we consider a rotation around y axis by an angle 2θ, such that $R = e^{-i\theta\sigma_y}$ (σ_y is the standard Pauli matrix in the y direction):

$$R(\theta) = \begin{pmatrix} \cos\theta & -\sin\theta \\ \sin\theta & \cos\theta \end{pmatrix}. \tag{3}$$

The operator R rotates the spin at each site, and then the spin-up component walks to the right, whereas the spin-down component walks the left. Such spin-dependent shift operation is implemented via the operator S:

$$S = \sum_{n=-\infty}^{\infty} (|n+1\rangle\langle n| \otimes |\uparrow\rangle\langle\uparrow| + |n-1\rangle\langle n| \otimes |\downarrow\rangle\langle\downarrow|), \tag{4}$$

where $|n\rangle$ refers to a ket state localized at site n, and $|\uparrow\rangle$ and $|\downarrow\rangle$ denote spin-up and spin-down states. The overall one-step quantum walk operator (without disorder) is then given by

$$U_{\rm DT} \equiv S\left(\sum_n |n\rangle\langle n| \otimes R\right). \tag{5}$$

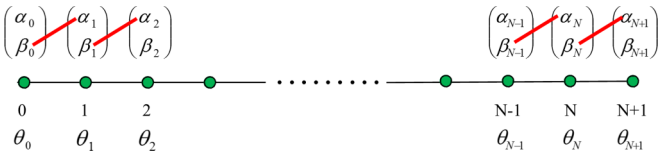

FIG. 1. (Color online) Set-up of our finite-chain QW with disorder, with totally $N+2$ sites, where site 0 and $N+1$ are the boundary sites with reflection operators R_- and R_+. Rotation operators of bulk sites with $n = 1,2\ldots N-1,N$ depend on the local angle θ_n, which fluctuate from site to site. The red slashes connect spin components β_n and α_{n+1}, as they form the new "spinor" in our transfer matrix formalism elaborated in our main text.

The above described QW can be restricted to a finite regime [20,51,52] through total-reflection coin operators $R_\pm$ at two boundaries, with $R_\pm$ defined as

$$R_\pm = \begin{pmatrix} 0 & \mp 1 \\ \pm 1 & 0 \end{pmatrix} = \begin{pmatrix} \cos(\pm\frac{\pi}{2}) & -\sin(\pm\frac{\pi}{2}) \\ \sin(\pm\frac{\pi}{2}) & \cos(\pm\frac{\pi}{2}) \end{pmatrix}. \tag{6}$$

Note that $R_\pm$ conserves the probability inside a finite QW chain and turns spin-down to spin-up, and vice versa. Since the coin operators at two boundaries can be either R_+ or R_-, we could have four choices of boundaries as $[R(\theta_0), R(\theta_{N+1})] = (R_\pm, R_\pm)$. In the following we mainly choose (R_-, R_+) as our boundary condition. Studies of other boundary conditions can be found in Appendix B. As depicted in Fig. 1, our QW model has totally $N+2$ sites, with N of them being bulk sites.

Next we introduce disorder to the QW model, by considering a perturbation to the local rotation angles θ_n, i.e.,

$$\theta_n = \tilde{\theta} + \delta_n \quad \text{for} \quad n = 1, 2, \ldots, N. \tag{7}$$

Here $\tilde{\theta}$ is identical for different sites n, while $\delta_n \in [-\Delta, \Delta]$ may differ from site to site (Δ is hence seen to be the amplitude of the box distributed random variable δ_n), giving rise to a disordered QW on a finite number of sites.

For such a finite-site QW system with a disordered bulk specified by θ_n, we can still define a mapping operator U, which can be obtained from the $U_{\rm DT}$ in Eq. (5) [that is, $R(\theta) \to \prod_n R(\theta_n)$]. In representation of different QW sites, U can be expressed explicitly as a $2(N+2) \times 2(N+2)$ matrix. As a mapping operator, U is unitary with eigenvalue $e^{i\omega}$:

$$U|\psi\rangle = e^{i\omega}|\psi\rangle, \tag{8}$$

where ω is the quasienergy eigenvalue of U, and $|\psi\rangle$ is the associated eigenstate characterized by

$$|\psi\rangle = (\alpha_0\ \beta_0\ \alpha_1\ \cdots\ \alpha_{N+1}\ \beta_{N+1})^{\rm T}, \tag{9}$$

with $(\cdots)^{\rm T}$ being the transpose operation. Because of the special choices of rotation operators at two boundaries, the first and last rows and the first and last columns of U have entries 0 only. Upon removing these rows and columns, U becomes a

$2(N+1)\times 2(N+1)$ matrix. Correspondingly, the entries α_0 and β_{N+1} in the eigenstate $|\psi\rangle$ can be also removed.

A. Transfer matrix formalism

In solving Eq. (8), one obtains the following recursive relation between the entries of the eigenstate $|\psi\rangle$:

$$\begin{aligned}\alpha_n e^{i\omega} &= \alpha_{n-1}\cos\theta_{n-1} - \beta_{n-1}\sin\theta_{n-1},\\ \beta_n e^{i\omega} &= \alpha_{n+1}\sin\theta_{n+1} + \beta_{n+1}\cos\theta_{n+1},\end{aligned} \tag{10}$$

with $n\in[1,N]$. Such relations can be expressed in the following matrix form:

$$\begin{pmatrix}\beta_n\\ \alpha_{n+1}\end{pmatrix} = T_n\begin{pmatrix}\beta_{n-1}\\ \alpha_n\end{pmatrix}, \tag{11}$$

with

$$T_n = \begin{pmatrix}e^{i\omega}\sec\theta_n & -\tan\theta_n\\ -\tan\theta_n & e^{-i\omega}\sec\theta_n\end{pmatrix}. \tag{12}$$

Here T_n is the transfer matrix [20] at site n.

In Eq. (11), the neighboring spinors' components β_{n-1} and α_n form the new "spinors" (See Fig. 1), and they are chained through local transfer matrices. Disordered parameter θ_n and quasienergy ω are contained in these matrices. This allows us to deal with disorder explicitly. This is one known advantage of the transfer matrix formalism (TMF) [53,54].

Given the chain relation between entries of the eigenstate $|\psi\rangle$ in Eq. (11), we still need to handle the boundary situations with care, i.e., $\binom{\beta_0}{\alpha_1}$ and $\binom{\beta_N}{\alpha_{N+1}}$. By setting n in Eq. (10) to be 0 and N, we obtain

$$\begin{aligned}\alpha_1 e^{i\omega} &= \alpha_0\cos\theta_0 - \beta_0\sin\theta_0,\\ \beta_N e^{i\omega} &= \alpha_{N+1}\sin\theta_{N+1} + \beta_{N+1}\cos\theta_{N+1},\end{aligned} \tag{13}$$

which further reduce to

$$\begin{pmatrix}\beta_0\\ \alpha_1\end{pmatrix} = c_0\begin{pmatrix}e^{i\omega}\\ -\sin\theta_0\end{pmatrix},\quad \begin{pmatrix}\beta_N\\ \alpha_{N+1}\end{pmatrix} = c_N\begin{pmatrix}\sin\theta_{N+1}\\ e^{i\omega}\end{pmatrix}. \tag{14}$$

Using the boundary conditions in Eq. (14), the chain relation in Eq. (11), as well as $\theta_0=-\pi/2$ and $\theta_{N+1}=\pi/2$, we finally obtain the following equation that carries all the information of Eq. (8):

$$c_N\begin{pmatrix}1\\ e^{i\omega}\end{pmatrix} = T_N\cdot T_{N-1}\cdot\cdots\cdot T_2\cdot T_1\cdot c_0\begin{pmatrix}e^{i\omega}\\ 1\end{pmatrix}. \tag{15}$$

For a specific realization of disorder, only particular values of the quasienergy ω satisfy Eq. (15). The coefficients c_N and c_0 can be determined from Eq. (15) and the normalization of $|\psi\rangle$.

To conclude, the TMF reduces a matrix equation with dimension $2(N+1)\times 2(N+1)$ [Eq. (8)] to a chained matrix equation connecting N matrices, each of dimension 2×2 [Eq. (15)]. This framework will be used later. Indeed, in the following we will not return to the original Eq. (8) but just focus on Eq. (15).

B. Special quasienergies and the implication of ODD

By observing the transfer matrix in Eq. (12), we notice that $\omega = 0, \pm\pi/2, \pi$ are special quasienergies. For example, when $\omega = 0$, the transfer matrix reduces to

$$T_n = \sec\theta_n\cdot\boldsymbol{I} - \tan\theta_n\sigma_x, \tag{16}$$

where σ_x is the Pauli matrix along the x direction and $\boldsymbol{I}$ is defined as the identity 2×2 matrix. Such simple transfer matrices can be exactly diagonalized in the basis of σ_x, so that the product of all the transfer matrices can be easily calculated. This being the case, whether $\omega = 0, \pm\pi/2$, or π satisfies Eq. (15) can be checked without difficulty. If ω is not equal to one of these special values, then it is virtually impossible to analytically check Eq. (15) because the product of these transfer matrices is hard to evaluate.

If ω assumes one of these special values, the corresponding eigenstates can be also analyzed in a straightforward manner. Take again the case of $\omega = 0$ as an example. When $\omega = 0$, from Eq. (16) we get

$$\begin{aligned}&\prod_{n=1}^{N} T_n = \frac{1}{2}(\lambda_+ + \lambda_-)\boldsymbol{I} + \frac{1}{2}(\lambda_+ - \lambda_-)\sigma_x,\\ &\text{with}\quad \lambda_+ = \lambda_-^{-1} = \prod_{n=1}^{N}\tan\left(\frac{\pi}{4} - \frac{\theta_n}{2}\right).\end{aligned} \tag{17}$$

The "spinors" at both ends of $|\psi\rangle$ are proportional to $\binom{1}{1}$, i.e., the eigenvector of σ_x, obtained from Eq. (14). Substituting Eq. (17) into Eq. (15), we get

$$\begin{pmatrix}1\\ 1\end{pmatrix} = \frac{c_0}{c_N}\lambda_+\begin{pmatrix}1\\ 1\end{pmatrix}, \tag{18}$$

which obviously holds by an appropriate choice of c_0/c_N. Therefore, $\omega = 0$ is indeed a quasienergy solution of the disordered QW system.

In Eq. (17), if θ_n fluctuates around 0 or π (i.e., $\tilde{\theta} = 0$ or π), $\ln|\lambda_+|$ will follow unbiased diffusion process around 0, so $|\lambda_+|\approx 1$ for large N, which means that exponential decay of the eigenstate $|\psi\rangle$ does not occur. This quantitative analysis resembles that of off-diagonal disordered TBM [21,22], so we suspect that our model also displays the physics of ODD. Indeed, later in Sec. III we will show that $\omega = 0$ is the localization-delocalization transition quasienergy, and Dyson's singularity emerges there, provided that θ_n takes values randomly from a box distribution $[-\Delta,\Delta]$. If θ_n fluctuates around values other than 0 or π, $|\lambda_+|$ will increase or decrease exponentially, resulting in the localized 0 or π mode, which we believe is related to those topologically protected edge states currently being studied [51].

In the rest of this paper, we focus on the quasienergy $\omega = 0$ and quasienergies in its vicinity. In Appendix C, we will discuss those cases with quasienergy values other than 0 or π.

III. PHYSICS OF ODD

As introduced in Sec. I, ODD for nearest-neighbor hopping is quite different from diagonal disorder and leads to peculiar properties. For our QW model, here we attempt to derive its DOS and localization length, keeping mind that it is possible for a delocalization transition to occur at some special quasienergy values. Here the random angles θ_n are assumed

to fluctuate in the interval $[-\Delta,\Delta]$ (i.e., $\tilde{\theta}=0$). The situation for $\tilde{\theta}=\pi$ is very analogous.

A. Analyzing quasienergy values

We start with Eq. (15) by considering its alternative form after some transformations:

$$\begin{pmatrix}1\\0\end{pmatrix}=c\begin{pmatrix}\cos\omega & i\sin\omega\\ i\sin\omega & \cos\omega\end{pmatrix}\cdot\boldsymbol{P}\cdot\begin{pmatrix}1\\0\end{pmatrix},\quad\text{with}$$
$$\boldsymbol{P}=\prod_{n=1}^{N}\left[\begin{pmatrix}\tan\vartheta_n & 0\\ 0 & \cot\vartheta_n\end{pmatrix}\begin{pmatrix}\cos\omega & i\sin\omega\\ i\sin\omega & \cos\omega\end{pmatrix}\right], \tag{19}$$

where $\vartheta_n=\frac{\pi}{4}-\frac{\theta_n}{2}$. The detailed derivation can be found in Appendix A. Note that if and only if ω takes the actual quasienergy value, then Eq. (19) will be satisfied. In particular, it is now obvious to observe from Eq. (19) that $\omega=0$ is one quasienergy value. To derive the DOS, we need to analyze other quasienergy values allowed by Eq. (19). To that end we first reinterpret Eq. (19), which is inspired by Schmidt's work [55] that treats spinors linked by transfer matrices as vectors in a plane.

Let us consider a complex plane with the x axis denoting the real part and the y axis denoting the imaginary part. In Eq. (19), the initial "spinor" $\binom{1}{0}$ can be treated as a vector lying in the real axis with length 1 pointing in the positive direction. So, from now on, we refer to the "spinor" as a "vector." Let

$$\widetilde{R}=\begin{pmatrix}\cos\omega & i\sin\omega\\ i\sin\omega & \cos\omega\end{pmatrix}\quad\text{and}\quad\widetilde{C}_n=\begin{pmatrix}\tan\vartheta_n & 0\\ 0 & \cot\vartheta_n\end{pmatrix}, \tag{20}$$

so $\widetilde{R}$ and $\widetilde{C}_n$ do the job of $\boldsymbol{P}$ in Eq. (19). Consider a vector $\mathbf{v}_n=\binom{x_n}{iy_n}$. Its angle with respect to positive x-axis is ϕ_n, and $\tan\phi_n=y_n/x_n$. According to Eq. (19), we define

$$\mathbf{v}_{n+1}=\widetilde{C}_n\cdot\widetilde{R}\cdot\mathbf{v}_n, \tag{21}$$

with $n=1,2,\ldots,N$ and $\mathbf{v}_1=\binom{1}{0}$. Hence, we can interpret Eq. (21) [and Eq. (19) thereafter] as the following (see also Fig. 2): $\widetilde{R}$ rotates vector $\mathbf{v}_n$ counterclockwise by an angle ω, followed by stretching in the x coordinate by a factor $\tan\vartheta_n$ and in the y coordinate by the factor $\cot\vartheta_n$ (due to $\widetilde{C}_n$), and then $\mathbf{v}_{n+1}$ is reached with the following relation:

$$\tan\phi_{n+1}=\tan(\phi_n+\omega)\cot^2\vartheta_n. \tag{22}$$

In Eq. (19), the initial vector $\mathbf{v}_i$ and final vector $\mathbf{v}_f$ are both $\binom{1}{0}$, and $\mathbf{v}_i=\mathbf{v}_1$, $\mathbf{v}_f=\widetilde{R}\cdot\mathbf{v}_{N+1}$, so $\tan\phi_1=\tan(\phi_{N+1}+\omega)=0$. As such, Eq. (19) presents such a physical picture: a vector initially located in the positive x axis is rotated and stretched or contracted, repeatedly, and after a final rotation, it lands back on the x axis. Therefore,

$$\phi_{N+1}+\omega=j\pi. \tag{23}$$

Note that ω has the period of 2π, so we assume $\omega\in[-\pi,\pi]$. Through interpreting Eq. (19) this way, we are now ready to derive the DOS near $\omega=0$. Without loss of generality, we consider a small positive quasienergy ω.

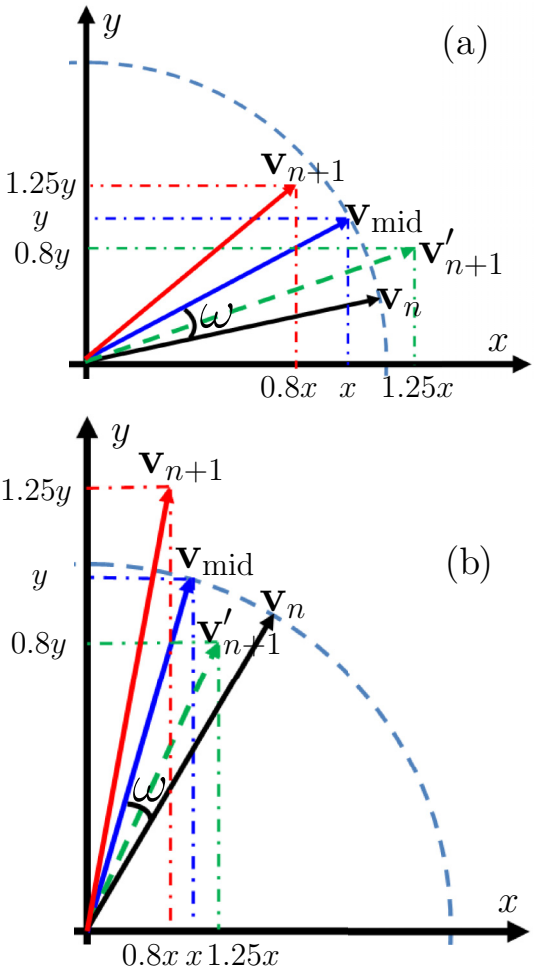

FIG. 2. (Color online) The operations in Eq. (19) illustrated via a complex plane with the x axis denoting the real part (the first component of the spinor) and the y axis denoting the imaginary part (the second component of the spinor). In the first quadrant, from top to bottom, the four vectors are $\mathbf{v}_{n+1}$, $\mathbf{v}_{\rm mid}$, $\mathbf{v}'_{n+1}$, and $\mathbf{v}_n$. $\widetilde{C}_n\cdot\widetilde{R}$ acts on $\mathbf{v}_n$ to get $\mathbf{v}_{n+1}$ (if contracted) or $\mathbf{v}'_{n+1}$ (if stretched). Specifically, $\widetilde{R}$ rotates $\mathbf{v}_n$ by angle ω to get $\mathbf{v}_{\rm mid}$; then $\widetilde{C}_n$ will stretch or contract $\mathbf{v}_{\rm mid}$. In panel (a), $\mathbf{v}_{\rm mid}$'s angle is less than $\pi/4$, while in panel (b) its angle is larger than $\pi/4$. Hence the length of $\mathbf{v}_{n+1}$ in panel (a) is smaller than in panel (b), whereas the opposite is true for $\mathbf{v}'_{n+1}$.

Regarding the rotating and stretching and contracting processes, there are two important factors to be noted. First, ϕ_n does not increase monotonically with respect to n. ϕ_{n+1} could be smaller than ϕ_n (see Fig. 2). However, ϕ_n has a tendency to increase because the positive ω forces $\mathbf{v}_n$ to rotate counterclockwise. Besides, a vector $\mathbf{v}_n$ can never cross x and y axes clockwise. For example, if $\mathbf{v}_n$ is inside the first quadrant, then $\tan\phi_n$ and $\cot^2\vartheta_n$ are positive, so for $\tan\phi_{n+1}$ in Eq. (22) to be negative (i.e., crossing the axis), $\tan(\phi_n+\omega)$ must be negative. Therefore, only the rotation $\widetilde{R}$ can bring a vector from one quadrant to another, while the stretching and contracting operation $\widetilde{C}_n$ cannot. The vector $\mathbf{v}_n$ can only drift away by crossing the positive y axis. Thus, in Eq. (23), j is always a positive integer. Second, in a single realization of disorder, the

following equation holds:

$$\phi_{N+1}(\omega_b) > \phi_{N+1}(\omega_a) \quad \text{for } \omega_b > \omega_a. \tag{24}$$

To prove this relation, we show that, given $\phi_n \geqslant \phi'_n$ and $\omega > \omega'$, then $\phi_{n+1} > \phi'_{n+1}$. We assume that ϕ_n and ϕ'_n are quite close and within the same quadrant, say the first quadrant. Then it is easy to see that

$$\begin{aligned}&\tan\phi_{n+1} - \tan\phi'_{n+1}\\ &\quad = [\tan(\phi_n + \omega) - \tan(\phi'_n + \omega')]\tan^2\vartheta_n > 0,\end{aligned} \tag{25}$$

so we get $\phi_{n+1} > \phi'_{n+1}$. This conclusion can be easily proved in other quadrants, too. Hence, starting with the same initial condition $\phi_1 = 0$ and same realization of disorder, after N cycles, the associated $\phi_{N+1}(\omega)$ is a monotonous function of ω. This feature is checked in our numerical studies.

Given the two factors above, we can now count the number of states between quasienergies 0 and ω. Suppose that the corresponding vector of ω sweeps an angle in between $j\pi$ and $(j+1)\pi$, then there exist j quasienergies $\omega_1 \cdots \omega_j$ that are the solution of the systems, and their vectors sweep angles $\pi \cdots j\pi$ correspondingly. Therefore, the number of states between 0 and ω is j, and, specifically,

$$\text{If} \quad j \leqslant \frac{\phi_N(\omega) + \omega}{\pi} < j + 1 \tag{26}$$

and

$$\begin{aligned}&\omega_1 < \omega_2 < \cdots < \omega_k < \cdots < \omega_{j-1} < \omega_j \leqslant \omega,\\ &\text{with} \quad k = \frac{\phi_{N+1}(\omega_k) + \omega_k}{\pi}.\end{aligned} \tag{27}$$

Here $k \in [1, j]$ and it is an integer. Next, we derive the integrated DOS from the total number of states.

B. Integrated density of states

The general form of the integrated DOS normalized over the number of sites is

$$N_I(\omega) = \int_{-\infty}^{\omega} \rho(\omega')d\omega'. \tag{28}$$

Here $\rho(\omega)$ is the density of state. In QW, due to a symmetry analyzed previously (see, e.g., [51]), the quasienergy ω is symmetric with respect to 0. There are an equal number of positive and negative quasienergy states so that $N_I(0) = 0.5$.

As shown in the previous section, the total number of states between quasienergies 0 and ω is j, and

$$j = [(\phi_{N+1}(\omega) + \omega)/\pi], \tag{29}$$

where $[x]$ denotes the largest integer less than or equal to x. So in our case,

$$N_I(\omega) - N_I(0) = \frac{j}{N+1}. \tag{30}$$

Now we need to evaluate j.

As shown in Eq. (21), $\mathbf{v}_{n+1}$ can be obtained from $\mathbf{v}_n$ after the operation $\widetilde{C}_n \cdot \widetilde{R}$. The initial vector $\mathbf{v}_i$ will experience totally $N+1$ operations to reach the final vector $\mathbf{v}_f$. To see this, we add a matrix $\widetilde{C}_{N+1}$ with $\vartheta_{N+1} = 0$ to the right of Eq. (19). It is the identity matrix so that Eq. (19) holds. From $\mathbf{v}_i$ to $\mathbf{v}_f$, the vector has passed many quadrants. We can define N_q to be the number of operations required for the vector to leave the qth quadrant since entering it. Obviously, the summation of all the N_q equals $N+1$: $\sum N_q = N+1$.

From $\mathbf{v}_i$ to $\mathbf{v}_f$, the vector rotates totally by an angle about $j\pi$ after $N+1$ operations [see Eq. (29)] so the number of quadrants passed is $2j$ and

$$\sum_{q=1}^{2j} N_q = 2j\left(\frac{1}{2j}\sum_{q=1}^{2j} N_q\right) = 2j\overline{N_q} = N+1. \tag{31}$$

Hence, we have this formula [22]:

$$N_I(\omega) - N_I(0) = j/(N+1) = \frac{1}{2\overline{N_q}}, \tag{32}$$

and $\overline{N_q}$ is the average number of operations required to pass one quadrant since entering it. Equation (32) resembles Eq. (21) in the paper by Eggarter and Riedinger [22]. Though we approach the DOS through counting the number of states, similar to what was done in Ref. [22], we are able to achieve this step by first introducing the transfer matrix approach when analyzing the spinors in our QW model. More importantly, because the above expression for counting the number of states is similar to that in Ref. [22], we can now analogously derive the DOS near $\omega = 0$.

C. Derivation of the DOS

In the previous subsection, the integrated DOS is derived in Eq. (32), but with one parameter $\overline{N_q}$ to be determined (which represents the average number of operations required to pass one quadrant). Without loss of generality, we consider the first quadrant.

Let $z_n \equiv \cot\phi_n$. From Eq. (22) we have

$$z_{n+1} = z_n \frac{1 - (\tan\omega)/z_n}{1 + z_n\tan\omega}\tan^2\vartheta_n. \tag{33}$$

We define $u_n \equiv \ln z_n$ for $z_n \neq 0$ or ∞. When

$$\tan\omega \ll z_n \ll (\tan\omega)^{-1}, \tag{34}$$

one approximately has

$$u_{n+1} \approx u_n + \ln(\tan^2\vartheta_n). \tag{35}$$

Since ϑ_n is taken randomly from this interval $[\pi/4 - \Delta, \pi/4 + \Delta]$, we can conclude that u_n executes a random walk [22]. One may notice that the fraction factor in Eq. (33) is always smaller than 1 for positive z_n, so the random walk in Eq. (35) is accompanied by a small negative drift. However, if the vector falls in the second quadrant, the fraction factor will be always larger than 1, such that the random walk has a small positive drift. The two drifts cancel each other approximately.

When u_n approaches the endpoints of the interval in (34), the approximation in (35) no longer holds. Here we analyze the situations upon approaching the endpoints to show that they are similar to the situations analyzed in Ref. [22]. If this is true, then the derivation there can be adopted here without much modification.

For $z_n \approx (\tan\omega)^{-1}$ (approaching the large z_n limit), then $z_{n+1} \approx (1/2)z_n\tan^2\vartheta_n$ according to Eq. (33). The net shrinking factor (1/2) in this expression indicates that z_{n+1} will not keep growing. So $u_{\max} = -\ln\tan\omega$ can be considered as the

reflection barrier as in Ref. [22]. We can also view the reflection as the manifestation that the vector can never cross the x axis clockwise (see Sec. III A.).

In the other extreme where $z_n \approx \tan\omega$ (approaching the small z_n limit), the numerator in Eq. (33) will be much smaller than 1 so that $z_{n+1} \ll z_n$, indicating a sharp decrease in z_n. Once z_n gets slightly below $\tan\omega$, z_{n+1} will be negative, indicating that the vector moves into the second quadrant. So this boundary $u_{\min} = \ln\tan\omega$ can be called an absorbing barrier [22]. The vector passes the positive y axis counterclockwise (see Sec. III A).

With all these, a mapping between our disordered QW model and the TBM with ODD is established regarding all the system parameters. Specifically, our Eqs. (32), (33) and (34) resemble Eqs. (21), (18), and (19) in Ref. [22], and the reflection and absorbing barriers are similar, too. Further borrowing the method in Sec. III of Ref. [22], we directly find $\overline{N_q}$:

$$\overline{N_q} = \frac{4\ln^2\tan\omega}{\sigma^2}, \quad \text{with} \quad \sigma^2 \equiv 2\langle(\ln\tan^2\vartheta)^2\rangle. \tag{36}$$

Using Eq. (32), we obtain the integrated DOS,

$$N_I(\omega) = \frac{1}{2}\left(1 + \frac{\sigma^2}{4\ln^2\tan\omega}\right), \tag{37}$$

and then the DOS,

$$\rho(\omega) = \frac{\mathrm{d}N_I}{\mathrm{d}\omega} \approx -\frac{\sigma^2}{4}\frac{1}{\omega\ln^3\omega}. \tag{38}$$

To conclude, we have shown that our disordered QW model possesses the physics of ODD. It is for this reason that, quite remarkably, the derivation of DOS for our QW model resembles that in the original TBM with ODD [21,22]. Making clear this connection between our QW model and the TBM with ODD is the main contribution of this section. We highlight the two crucial steps: (i) linking the "spinor" components of the eigenstate through the transfer matrices and (ii) the interpretation of the eigenstate as a vector moving in the complex plane when counting the number of states.

The localization length for quasienergies around 0 can be derived in a similar way [22], and the result is

$$\ell^{-1}(\omega) \approx -\frac{\sigma^2\ln\omega}{4\ln^2\tan\omega} \approx -\frac{\sigma^2}{4\ln\omega}. \tag{39}$$

Equation (39) shows that the localization length diverges as ω approaches 0, which is consistent with the previously mentioned fact that the state with $\omega = 0$ is delocalized.

D. Numerical analysis of the DOS

The derivation of DOS in Sec. III C involves some approximations, so we need numerical simulations to check the analytical results. Specifically, we use Eqs. (22), (29), and (30) to obtain the integrated DOS numerically, and then compare our numerics with the analytical expression given by Eq. (37). Given one disorder realization and one quasienergy ω, we use the recursive relation in Eq. (22) to obtain ϕ_{N+1}, and then it is substituted into Eq. (29) to obtain j, and finally we get $N_I(\omega)$ through Eq. (30). Note that a randomly chosen ω may not be an actual quasienergy value associated with a particular disorder realization. However, if the system is sufficiently large, the quasienergy values will cover the vicinity of 0 quite densely. For this reason, a randomly chosen ω will not cause noticeable error in terms of the counting of states.

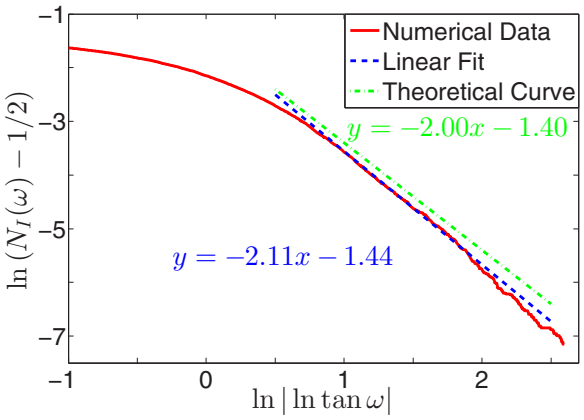

FIG. 3. (Color online) Relation between integrated DOS and quasienergy ω, shown via $\ln(N_I(\omega) - \frac{1}{2})$ as a function of $\ln|\ln\tan\omega|$. The QW chain is of size $N = 3 \times 10^4$. The (red) solid line is from direct numerical calculations, the (blue) dashed line is a linear fit, and the (green) dash-doted line is our theoretical curve. The linear fit is applied to the domain $\ln|\ln\tan\omega| \in [1,2]$, corresponding to the quasienergy domain $\omega \in [6.18 \times 10^{-4}, 6.60 \times 10^{-2}]$.

The analytical relation between $N_I(\omega)$ and ω is given by Eq. (37). Alternatively,

$$\ln\left(N_I(\omega) - \frac{1}{2}\right) = \ln\frac{\sigma^2}{8} - 2\ln|\ln\tan\omega|. \tag{40}$$

Figure 3 depicts $\ln(N_I(\omega) - \frac{1}{2})$ as a function of $\ln|\ln\tan\omega|$ to check this theoretical prediction. The theoretical intersection on the y axis is $\ln\frac{\sigma^2}{8} \approx -1.40$ and the slope of the curve is -2. Our numerical results agree with theory well in the main domain of our interest. However, for ω larger than $e^{-e} \approx 0.066$ (equivalently, $\ln|\ln\tan\omega| < 1$), theoretical results deviate from the numerical data, implying the failure of the analytical approximations made in Sec. III C. This is expected as a too large ω leads to errors in Eq. (34) and then in Eq. (35). In the case of $\omega < e^{-e^2} \approx 6.18 \times 10^{-4}$ (equivalently, $\ln|\ln\tan\omega| > 2$), the system size N is no longer large enough for a reliable statistical analysis, so the corresponding numerical results also start to deviate from our theoretical predictions.

E. A numerical study of the self-correlation of delocalized states

Here we numerically check whether the average two-point correlation of a delocalized state with $\omega = 0$ decays polynomially. We use many realizations of disorder to obtain an average correlation function. This is different from our previous calculations where only a single realization of disorder is needed. Analytically, assuming that a dimensionless product of disorder strength and two-point separation is much larger than unity [28], the correlation exponent is shown to be $-3/2$. This theoretical prediction is checked here by use of

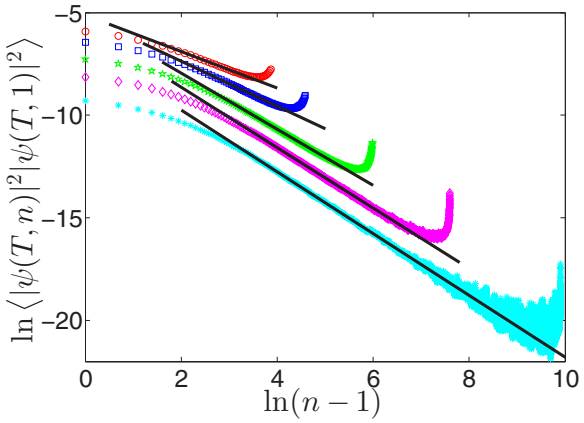

FIG. 4. (Color online) Dependence of correlation on the system size with the disorder strength fixed, as shown by $\ln\langle|\psi(n)|^2|\psi(1)|^2\rangle$ vs $\ln(n-1)$, averaging over 1 000 000 disorder realizations. Here $|\psi(n)|^2$ is the probability of the wave function at site n, and $\langle|\psi(n)|^2|\psi(1)|^2\rangle$ is the averaged two-point correlation, with one point fixed to be the site 1. From top to bottom, the system size is set to be $N = 50$, 100, 400, 2000, and 20 000, respectively, and the linear fitting curves have slopes -0.89, -1.09, -1.36, -1.47, and -1.50. The disorder strength is fixed to be $\Delta = 0.4$.

Eqs. (17) and (18), which depicts the eigenstate structure of our disordered QW model.

In Fig. 4, the disorder strength is set to be $\Delta = 0.4$, and the system size varies from $N + 2 = 52$ to 20 002. When the two-point separation increases, the correlation exponent increases from 0.8 to 1.5 and stays almost stable at 1.5. Figure 5 shows how the correlation varies with the disorder strength. The general observation is that increasing the disorder strength

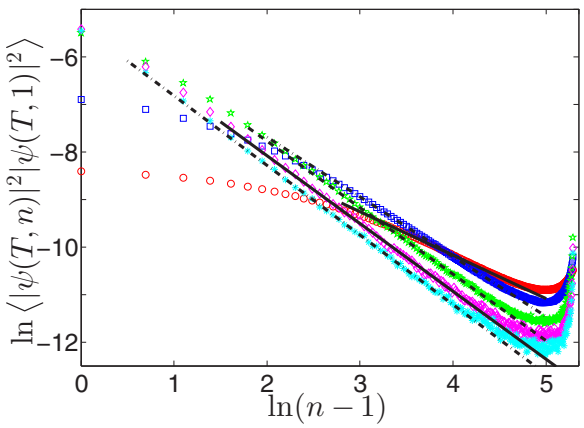

FIG. 5. (Color online) Dependence of correlation on disorder strength with the system size fixed, as shown by $\ln\langle|\psi(n)|^2|\psi(1)|^2\rangle$ vs $\ln(n-1)$, averaging over 1 000 000 disorder realizations. $|\psi(n)|^2$ is the probability of wave function at site n. System size $N + 2 = 202$. Symbols (red) circle, (blue) square, (green) polygon star, (magenta) diamond and (cyan) star represent $\Delta = 0.2$, 0.4, 1.0, 1.4, and 1.56, respectively. The associated linear fitting curves (solid, dash-dot, dash, solid and dash-dot lines) give slopes -0.91, -1.26, -1.50, -1.42, and -1.46, clearly indicating a saturation behavior at about $-3/2$ as the disorder strength increases.

will increase the correlation exponent, but the exponent again tends to saturate around $-3/2$. These numerical results are consistent with the early theoretical prediction of ODD [27,28]. However, we point out that if N and Δ are too large, the statistical fluctuations become more pronounced due to our finite number of realizations of disorder.

IV. EXPERIMENTAL PREPARATION OF THE 0 MODE IN DISORDERED QW

It is now clear that when the disordered local rotation angle variables θ_n fluctuate around zero [i.e., $\tilde{\theta} = 0$ in Eq. (7)], then the 0 mode (eigenstate with $\omega = 0$) in our disordered QW model reflects the physics of ODD. However, if $\tilde{\theta} \neq 0$, then the corresponding 0 mode becomes unrelated to ODD physics. For example, if θ_n slightly fluctuates around $\pi/2$, then the 0 mode will still be highly localized around the sites 0 and 1, with negligible proportion in all other sites.

The 0 mode with $\tilde{\theta} = 0$ is in general delocalized and hence it is hard to prepare in experiments. To address this issue, we note that the highly localized 0 mode associated with $\tilde{\theta} = \pi/2$ is a good starting point. We propose to connect this localized 0 mode with our target 0 mode possessing ODD physics by an adiabatic protocol [56–58]. That is, by slowly tuning the value of $\tilde{\theta}$ from $\pi/2$ to 0, we may reach our target 0 mode from the localized 0 mode.

Consider then a conventional adiabatic evolution protocol, through which the parameters θ_n in the QW operator U are tuned slowly. Note, however, that the boundary rotation angles θ_0 and θ_{N+1} must be fixed to ensure the conservation of probability inside the QW chain. An adiabatic process reflecting this constraint is as follows. At first, the system is set as $\theta_0 = -\pi/2, \theta_1 = \theta_{N+1} = \pi/2$ and $\theta_n = \pi/2 + \delta_n$ with $n \in [2, N]$ and δ_n being random angle fluctuations. The mean value of δ_n over N sites is denoted $\bar{\delta}$. The initial state of the QW model is prepared with entries $\beta_0 = \alpha_1 = 1/\sqrt{2}$ and all other entries 0. It can be easily checked that this initial state is precisely the 0 mode of the system (note that θ_1 is chosen to be $\pi/2$). Then, we slowly reduce θ_n during the QW process, until $\theta_n = \delta_n$. To be more specific, the proposed adiabatic protocol can be achieved by introducing a slow time dependence to $\tilde{\theta}$ in Eq. (7), i.e.,

$$\theta_n(t) = \tilde{\theta}(t) + \delta_n, \tag{41}$$

with $n \in [1, N]$ denoting the bulk-site index, $\delta_1 = 0$, and $\tilde{\theta}(t)$ to be further specified below.

The QW mapping operator U associated with $\theta_n(t)$ is denoted as $U(t)$. The initial state $|\psi(0)\rangle$ is localized at the first two sites, with $U(0)|\psi(0)\rangle = |\psi(0)\rangle$. The time-evolving state at time t is denoted $|\psi(t)\rangle$, obtained by

$$|\psi(t)\rangle = U(t) \cdot U(t-1) \cdot \cdots \cdot U(1) \cdot U(0)|\psi(0)\rangle. \tag{42}$$

For the sake of comparison between the time evolving state $|\psi(t)\rangle$ and our target 0 mode state, we define the exact zero-quasienergy eigenstate of $U(t)$ as $|\psi^0(t)\rangle$ (with $U(t)|\psi^0(t)\rangle = e^{i\cdot 0}|\psi^0(t)\rangle$). Numerically we can directly diagonalize $U(t)$ to get $|\psi^0(t)\rangle$. Our hope is to reach $|\psi^0(t)\rangle$ through the time evolving state $|\psi(t)\rangle$ emerging from our adiabatic protocol. Indeed, the adiabatic theorem [56–58] states that $|\psi(t)\rangle \approx |\psi^0(t)\rangle$ if the adiabatic conditions are fulfilled.

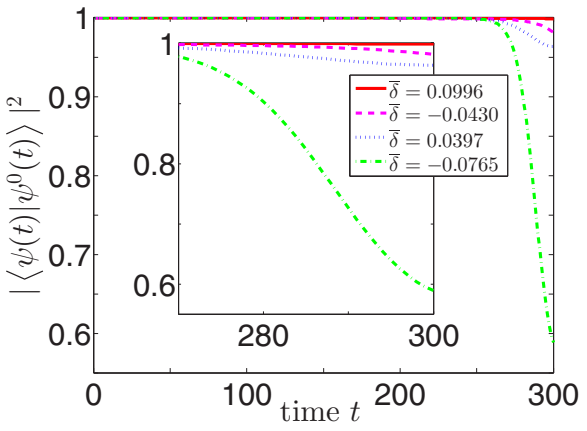

FIG. 6. (Color online) Overlap probability between the actual time evolving state $|\psi(t)\rangle$ and instantaneous 0 modes $|\psi^0(t)\rangle$ for four realizations of disorder in numerical experiments. The inset is a magnified view of the tail part. The (red) solid, (pink) dashed, (blue) dotted, and (green) dash-dotted lines represent four different realizations of disorder with different $\overline{\delta}$ (shown on the figure panel). The disordered chain has totally $N+2=20$ sites, with the disorder strength given by $\Delta = 0.7$.

We have numerically simulated the process depicted in Eq. (42), and then compare $|\psi(t)\rangle$ with $|\psi^0(t)\rangle$. Their overlap probabilities $|\langle\psi(t)|\psi^0(t)\rangle|^2$ vs t are plotted to check the performance of a certain specific protocol. In the following, by specifying $\tilde{\theta}(t)$ differently, we examine two protocols to realize the adiabatic process and hence the preparation of the target 0 mode state that reflects the physics of ODD.

A. Tuning $\tilde{\theta}$ at a constant rate

In this case we decrease the bulk θ_n at a constant rate with respect to the evolution time. Specifically, $\tilde{\theta}(t)$ in Eq. (41) is given by

$$\tilde{\theta}(t) = \tilde{\theta}(0) - rt, \tag{43}$$

where $t = 0,1,2,\ldots,T$ is the evolution time, $r = \tilde{\theta}(0)/T$ is the constant decreasing rate, and $\tilde{\theta}(0) = \pi/2$. The obtained state fidelity $|\langle\psi(t)|\psi^0(t)\rangle|^2$ vs t is plotted in Fig. 6.

Figure 6 shows that, for some realizations of disorder, the fidelity near the final stage of the evolution decreases significantly. The difference seems to be related to $\overline{\delta}$, the actual mean value of the random fluctuations δ_n in particular realizations of disorder. For example, the realization with $\overline{\delta} \approx -0.076$ (green dash-dotted line) has a final fidelity below 0.6. To understand this, we investigate the gap between the 0 mode and its neighboring mode, which is found to decrease with t (the gap is calculated by diagonalizing the instantaneous quantum walk operator U at particular times). When $\tilde{\theta}(t)$ gets close to 0, the 0 mode is not well separated from the bulk modes, and the gap becomes quite small. Compared with other three realizations, the realization with $\overline{\delta} \approx -0.076$ has a gap size of approximately half of others from $t \approx 250$ to 300, so this small gap has caused the most pronounced nonadiabatic transitions. To confirm this, we increase the total evolution time and indeed a better performance can be obtained (see Fig. 8 presented later). In contrast, for other realizations in Fig. 6, the final fidelity is high (above 0.95), an indication of good performance due to the associated relatively large gaps. To summarize, the performance of this adiabatic protocol is determined by the total evolution time T and the gap size in the final evolution stage. One can always improve the performance by increasing T. In contrast, the gap size is sensitive to the details of an actual realization of disorder. As an observation from our numerical results, cases with a negative $\overline{\delta}$ tend to have a smaller gap size around the final evolution stage than cases with a positive $\overline{\delta}$ (note, this seems to be the trend and we did not check all realizations).

B. Tuning $\tilde{\theta}$ exponentially

To understand our motivation of this alternative protocol, we first discuss the gap size of the clean system, where the bulk θ_n is uniform (i.e., $\theta_n = \tilde{\theta}$). In this case, two quasienergy bands emerge and the dispersion relation is given by $\cos\omega = \cos\tilde{\theta}\cos k$ [51], where k is the quasimomentum. The gap between the bands is $2\tilde{\theta}$ at $k = 0$. The 0 mode sits in the center of the band gap. We are thus motivated to design the following protocol by roughly assuming that the gap between the 0 mode and the bulk spectrum is proportional to $\tilde{\theta}$:

$$\frac{\mathrm{d}}{\mathrm{d}t}\tilde{\theta}(t) = -\lambda\tilde{\theta}(t). \tag{44}$$

In this new protocol, the rate of change $\frac{d}{dt}\tilde{\theta}(t) \propto$ instantaneous gap $\propto$ instantaneous $\tilde{\theta}(t)$. As the gap decreases, the rate of change also decreases to keep the process being sufficiently adiabatic. Therefore $\tilde{\theta}$ is an exponential function of t,

$$\tilde{\theta}(t) = \tilde{\theta}(0)e^{-\lambda t}, \tag{45}$$

where λ is the exponential decay rate of $\tilde{\theta}$. Using this protocol, θ_n can be explicitly expressed as a function of t:

$$\theta_n(t) = \begin{cases} -\frac{\pi}{2}, & n = 0, \\ \tilde{\theta}(t), & n = 1, \\ \tilde{\theta}(t) - \frac{N}{N-1}\tilde{\theta}(T) + \delta_n, & n \in [2,N], \\ \frac{\pi}{2}, & n = N+1. \end{cases} \tag{46}$$

Here $\frac{N}{N-1}\tilde{\theta}(T)$ is to make sure that $\sum_{n=1}^{N}\theta_n(t) = \sum_{n=1}^{N}\delta_n$ at the final time $t = T$. Note also that at site $n = 1$, $\theta_1(0) = \tilde{\theta}(0) = \pi/2$, which ensures that the initial 0 mode is the exact eigenstate of the QW propagator at time zero.

Figure 7 shows the performance of this protocol. For positive $\overline{\delta}$, the overlap probability at final time is quite high (above 0.998). Interestingly, similar to the previous protocol in which we sweep $\tilde{\theta}$ at a constant rate, the fidelity degrades in cases of $\overline{\delta} < 0$. In addition, in some realizations of disorder, the gap size may be erratic during the last stage of the adiabatic protocol, especially when $\overline{\delta}$ turns from positive to negative. This explains the relatively poor performance for the case with $\overline{\delta} = -0.108$ in Fig. 7.

Nevertheless, we can further improve the fidelity by increasing the total evolution time T or decreasing λ in our exponential protocol. Panel (a) of Fig. 8 shows fidelity changes with T. As a comparison, in panel (b) of Fig. 8 we show the parallel fidelity vs T if $\tilde{\theta}$ is swept at a constant rate. It is seen

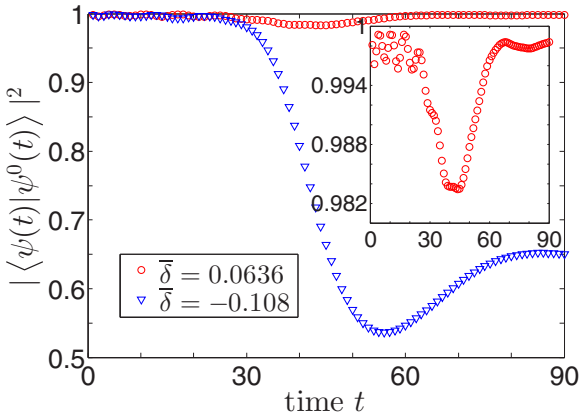

FIG. 7. (Color online) Overlap probability between the actual time evolving state $|\psi(t)\rangle$ and instantaneous 0 modes $|\psi^0(t)\rangle$ for two different types of disorder realization. The chain has $N+2=20$ sites, total evolution time $T=90$, disorder strength $\Delta=0.7$, and the parameter in the exponential protocol is characterized by $\lambda=0.0562$. (Red) Circles are for a case with the averaged angular disorder $\overline{\delta}=0.064$ being positive, with the overlap probability above 0.998 at the final time. The inset shows more details. (Blue) Triangles are for a case with the averaged angle disorder $\overline{\delta}=-0.108$ being negative. In this case, the final overlap probability is only around 0.65, which means that this protocol is still not working well with $T=90$.

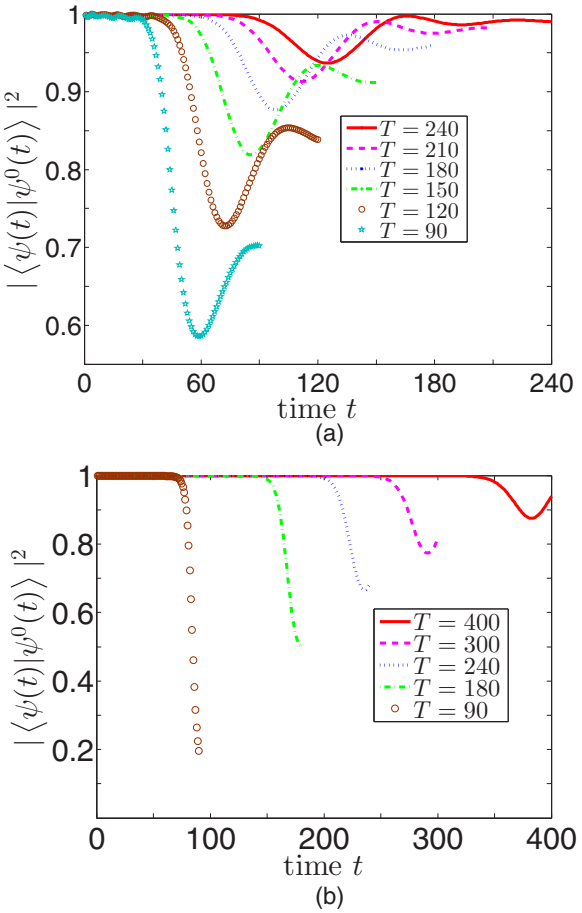

FIG. 8. (Color online) Overlap probability vs t for different protocol duration T, for an exponential protocol (a) [Eq. (45)] and the previous constant-rate protocol (b). In both protocols, the disorder realization is the same as the one with $\overline{\delta}=-0.1083$ in Fig. 7, and $N+2=20, \Delta=0.7$. (a) From top to bottom, T equals 240, 210, 180, 150, 120, and 90. The corresponding values of λ is chosen to be $\lambda=-\ln[0.01/(\pi/2)]/T$. (b) From top to bottom, T equals 400, 300, 240, 180, and 90. In both panels, a larger T results in a better fidelity of the final state. However, the exponential protocol in general requires less time to achieve the same fidelity.

that, overall, tuning $\tilde{\theta}$ exponentially as is done here is much better than tuning $\tilde{\theta}$ at a constant rate.

C. Correlation exponents in numerical experiments

We have shown in the previous subsection how to prepare the 0 mode state possessing the physics of ODD. Here we aim to show that states prepared in this manner can indeed manifest the correlation exponent characteristic of ODD physics. In doing so we need to perform averaging over many realizations of disorder. We use the exponential adiabatic protocol in our numerical experiment. To benchmark our numerical experiments, we also analyze the correlation exponent using the exact delocalized 0 mode state obtained from Eqs. (17) and (18).

Before presenting our results, we first discuss two minor issues. The first is related to the fact that the spinors represented in Fig. 1 involve two different sites. That is, In a real experiment, what is measured is likely the probability at each site, whereas in our analytical study, we treat $(\beta_{n-1}\ \alpha_n)^{\mathrm{T}}$ as one "spinor." However, we find that this difference has little effect on the correlation exponent. The other issue is that we have fixed θ_1 to be $\pi/2$ (hence not random) (see Sec. IV for details). Again, it is checked that this does not affect our analysis.

We also note that the $-3/2$ correlation exponent was derived under the assumption that the product of the dimensionless disorder strength and two-point separation is much larger than unity [28]. In real experiments, the QW chain might not be long, so we are limited to relatively small two-point separation. That means we should choose strong disorder strength to fulfill this assumption. Figure 9 presents our results from numerical experiments based on an exponential adiabatic protocol starting from a highly localized state, as compared with a direct investigation using the exact delocalized 0-mode states. For two different chain length, the two-point correlation exponents in our numerical experiments are found to be -1.48 and -1.36, as compared with -1.6 and -1.5 obtained from pure theory. Certainly, the agreement between these two sets of data can be further improved if we further increase T. The conclusion is that our adiabatic protocol applied to our disordered QW model is also useful in the actual demonstration of the two-point correlation characteristic of ODD physics.

For small systems with weak disorder, the analytical correlation exponents are not available [28]. To motivate experimental studies on this matter, below we further exploit our setup to investigate how the two-point correlation changes with weak disorder strength Δ and system size $(N+2)$.

We choose four different system sizes with a fixed and weak disorder strength $\Delta=0.4$. In particular, we let $N+2=12$,

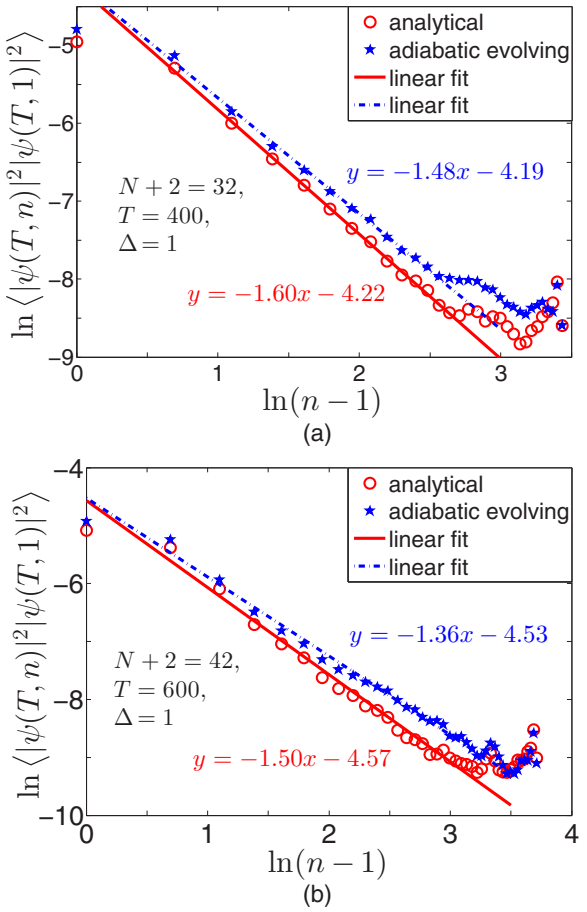

FIG. 9. (Color online) Correlation function $\ln\langle|\psi(T,n)|^2|\psi(T,1)|^2\rangle$ vs $\ln(n-1)$, averaged over 1000 disorder realizations. (a) Disorder strength $\Delta = 1$, system size $N + 2 = 32$; (b) $\Delta = 1$, $N + 2 = 42$. The total evolution time T is chosen to assure satisfactory fidelity in the adiabatic preparation of the 0 mode, with $T = 400$ in panel (a) and $T = 600$ in panel (b). In both panels (red) circles denote results from solving the 0 mode analytically; whereas (blue) stars denote results obtained from our adiabatic preparation of the 0 mode with the exponential protocol. Solid line and dash-dotted line are the associated linear fitting curves over a regime without much fluctuation. The slopes of the fitting curves reflect the correlation exponents.

22, 32, and 42. The results are shown in Fig. 10. For each case, we show statistical results obtained from analytical treatment of the 0 mode with disorder and from our exponential adiabatic protocol that starts from an initial localized state. The results obtained from such two totally different methods agree very well because they yield almost the same slopes from the fitting straight lines, for all the four cases shown. The good fitting by the straight lines indicates a polynomial behavior of the two-point correlation function, but now with correlation exponents given by -0.447, -0.588, -0.645, and -0.769, for $N = 10$, 20, 30, and 40, respectively. These exponents are far from $-3/2$, but show a tendency to approach $-3/2$ as the system size increases. Further increasing the value of Δ also increases the magnitude of the correlation exponent. These results should be of experimental interest as well and invite further theoretical developments in studies of the physics of ODD.

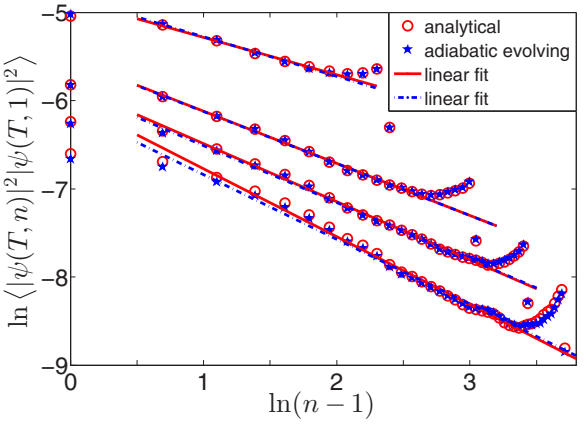

FIG. 10. (Color online) Correlation functions with weak disorder in a QW model, shown via $\ln\langle|\psi(T,n)|^2|\psi(T,1)|^2\rangle$ vs $\ln(n-1)$, averaged over 1000 disorder realizations. The total evolution time T is chosen to make sure the adiabatic protocol can yield a satisfactory fidelity of the 0-mode state. For example, if Δ or N is increased, T is increased also (See Sec. IV B). Here $\Delta = 0.4$, and from top to bottom the system size is $N + 2 = 12$, 22, 32, and 42 respectively. The slopes of the curves fitting the results using the exact 0 mode (red solid line) are -0.45, -0.59, -0.65, and -0.77, whereas the slopes of the curves fitting the results arising from our adiabatic protocol (blue dash-dotted line) are -0.42, -0.59, -0.66, and -0.73 respectively. The symbols and the lines share the same meaning with those in Fig. 9.

V. SUMMARY

To summarize, we have shown that the physics of ODD can be investigated by a disordered QW model. The associated exotic features in the delocalization and in the wave-function correlation are derived and numerically verified. Because the physics of ODD is rarely cleanly observed in actual experiments, our results will possibly motivate ongoing QW experiments as a new platform to study the physics of ODD. To facilitate such efforts, we proposed and analyzed adiabatic protocols to prepare the exotic delocalized 0-mode state with good fidelity. Our numerical experiments show that the delocalized 0-mode states thus obtained can directly show the correlation exponent $-3/2$ in the regime predicted by existing theory. Our numerical experiments also show that much different correlation exponents emerge if the product of the system size and the disorder strength is relatively small.

APPENDIX A: FROM EQ. (15) TO EQ. (19)

Here we show how to derive Eq. (19) from Eq. (15). Multiply both sides of Eq. (15) with $e^{-i\frac{\omega}{2}}$, and decompose T_n using the identity

$$T_n = \begin{pmatrix} e^{i\omega}\sec\theta_n & -\tan\theta_n \\ -\tan\theta_n & e^{-i\omega}\sec\theta_n \end{pmatrix} \equiv \begin{pmatrix} e^{i\frac{\omega}{2}} & 0 \\ 0 & e^{-i\frac{\omega}{2}} \end{pmatrix} \begin{pmatrix} \sec\theta_n & -\tan\theta_n \\ -\tan\theta_n & \sec\theta_n \end{pmatrix} \begin{pmatrix} e^{i\frac{\omega}{2}} & 0 \\ 0 & e^{-i\frac{\omega}{2}} \end{pmatrix}, \quad \text{(A1)}$$

then Eq. (15) becomes

$$\begin{pmatrix} e^{-i\frac{\omega}{2}} \\ e^{i\frac{\omega}{2}} \end{pmatrix} = c \begin{pmatrix} e^{i\frac{\omega}{2}} & 0 \\ 0 & e^{-i\frac{\omega}{2}} \end{pmatrix} \begin{pmatrix} \sec\theta_N & -\tan\theta_N \\ -\tan\theta_N & \sec\theta_N \end{pmatrix} \cdot \begin{pmatrix} e^{i\omega} & 0 \\ 0 & e^{-i\omega} \end{pmatrix} \begin{pmatrix} \sec\theta_{N-1} & -\tan\theta_{N-1} \\ -\tan\theta_{N-1} & \sec\theta_{N-1} \end{pmatrix} \vdots \cdot \begin{pmatrix} \sec\theta_1 & -\tan\theta_1 \\ -\tan\theta_1 & \sec\theta_1 \end{pmatrix} \begin{pmatrix} e^{i\frac{\omega}{2}} & 0 \\ 0 & e^{-i\frac{\omega}{2}} \end{pmatrix} \begin{pmatrix} e^{i\frac{\omega}{2}} \\ e^{-i\frac{\omega}{2}} \end{pmatrix}. \tag{A2}$$

Replace $\binom{e^{-i\frac{\omega}{2}}}{e^{i\frac{\omega}{2}}}$ and $\binom{e^{i\frac{\omega}{2}}}{e^{-i\frac{\omega}{2}}}$ in Eq. (A2) with the identities

$$\begin{pmatrix} e^{-i\frac{\omega}{2}} \\ e^{i\frac{\omega}{2}} \end{pmatrix} \equiv \begin{pmatrix} e^{-i\frac{\omega}{2}} & 0 \\ 0 & e^{i\frac{\omega}{2}} \end{pmatrix} \begin{pmatrix} 1 \\ 1 \end{pmatrix}, \quad \begin{pmatrix} e^{i\frac{\omega}{2}} \\ e^{-i\frac{\omega}{2}} \end{pmatrix} \equiv \begin{pmatrix} e^{i\frac{\omega}{2}} & 0 \\ 0 & e^{-i\frac{\omega}{2}} \end{pmatrix} \begin{pmatrix} 1 \\ 1 \end{pmatrix}. \tag{A3}$$

Equation (A2) then becomes

$$\begin{pmatrix} 1 \\ 1 \end{pmatrix} = c \begin{pmatrix} e^{i\omega} & 0 \\ 0 & e^{-i\omega} \end{pmatrix} \cdot \prod_{n=1}^{N} \left[\begin{pmatrix} \sec\theta_n & -\tan\theta_n \\ -\tan\theta_n & \sec\theta_n \end{pmatrix} \begin{pmatrix} e^{i\omega} & 0 \\ 0 & e^{-i\omega} \end{pmatrix} \right] \begin{pmatrix} 1 \\ 1 \end{pmatrix}. \tag{A4}$$

Multiply matrix P^{-1} from the left of both sides of Eq. (A4) and insert the identity $I = P^{-1}P$ between neighboring matrices in the right-hand side, where $P^{-1} = P = (\sigma_x + \sigma_z)/\sqrt{2}$, we will arrive at Eq. (19) because

$$P^{-1} \begin{pmatrix} e^{i\omega} & 0 \\ 0 & e^{-i\omega} \end{pmatrix} P = \begin{pmatrix} \cos\omega & i\sin\omega \\ i\sin\omega & \cos\omega \end{pmatrix}, \quad P^{-1} \begin{pmatrix} \sec\theta_n & -\tan\theta_n \\ -\tan\theta_n & \sec\theta_n \end{pmatrix} P = \begin{pmatrix} \tan\vartheta_n & 0 \\ 0 & \tan\vartheta_n \end{pmatrix}, \tag{A5}$$

where $\vartheta_n = \frac{\pi}{4} - \frac{\theta_n}{2}$.

APPENDIX B: MORE ON THE BOUNDARY CONDITIONS

Previously we employ one specific boundary condition to study the physics of ODD, but leave three other boundary conditions unexplored. Here we will briefly summarize the special quasienergies and the corresponding states [51,52] for these different boundary conditions.

Given the bulk $\theta_n = \pi/4 + \delta_n$ with $|\delta_n| < \pi/4$, then the boundary condition $(\theta_0,\theta_{N+1}) = (-\pi/2,\pi/2)$ $[(\pi/2, -\pi/2)]$ will lead to the edge states with quasienergy $\omega = 0$ or π localized around the boundary site $n = 0$ $f[n = N + 1]$. For convenience, we assume $\delta_n = 0$ in our qualitative discussions below.

Interestingly, the 0 or π quasienergy states are absent under the boundary conditions $(\theta_0,\theta_{N+1}) = (\pi/2,\pi/2)$. For the case of $(\theta_0,\theta_{N+1}) = (-\pi/2, -\pi/2)$, it can be shown that there exist localized edge states with quasienergies slightly differing from 0 or π. These features are also relevant to understand the topological properties in QW [51,52]. Here we elaborate these features using the transfer matrix formalism (TMF). Following the same method in Sec. III, the relation between two boundaries given by Eq. (15) can be written in the form analogous to Eq. (19):

$$\begin{pmatrix} 1 \\ 0 \end{pmatrix} = c_a \begin{pmatrix} \cos\omega & i\sin\omega \\ i\sin\omega & \cos\omega \end{pmatrix} \cdot \boldsymbol{P} \cdot \begin{pmatrix} 0 \\ i \end{pmatrix}, \tag{B1}$$

$$\begin{pmatrix} 0 \\ i \end{pmatrix} = c_b \begin{pmatrix} \cos\omega & i\sin\omega \\ i\sin\omega & \cos\omega \end{pmatrix} \cdot \boldsymbol{P} \cdot \begin{pmatrix} 1 \\ 0 \end{pmatrix}. \tag{B2}$$

Here $\vartheta_n = \frac{\pi}{4} - \frac{\theta_n}{2}$ and $\boldsymbol{P}$ is given in Eq. (19). Equation (B1) is for the boundary condition $(\theta_0,\theta_{N+1}) = (\pi/2,\pi/2)$ and Eq. (B2) is for $(\theta_0,\theta_{N+1}) = (-\pi/2, -\pi/2)$.

In the case of Eq. (B1) and using the same language as in Sec. III A, an actual quasienergy ω needs to bring a vector initially at the y axis, $\binom{0}{i}$, to the x axis, $\binom{1}{0}$. For simplicity, we assume the vector goes from the positive y axis to the negative x axis. $\omega = 0$ or π certainly cannot accomplish this task since it will let the vector stay in the y axis. Let us check if a small value ϵ which slightly above 0 can be the quasienergy, using Eq. (22) with $\theta_n = \pi/4, \phi_1 = \pi/2, \phi_N = \pi - \epsilon$, and $\vartheta_n = \pi/8$. It then follows that $\tan\phi_n$ should approach 0 from $-\infty$ (that is, after the vector enters the second quadrant). However, this cannot be true since $\cot^2(\pi/8) \gg 1$ will prevent $\tan\phi_n$ from approaching 0. Together with other simple considerations, it is seen that, under the above boundary condition, $\omega = 0,\pi$ and any value near them cannot be the quasienergies of the system.

In the case of Eq. (B2), the vector should go from the x axis to the y axis. For simplicity, we assume the vector goes from the positive x axis to the positive y axis. This corresponds to $\tan\phi_n$ going from 0 to ∞. It is obvious that $\omega = 0$ or π cannot achieve this goal. Again we consider a small value $\omega = \epsilon$. Now the factor $\cot^2(\pi/8) \gg 1$ in Eq. (22) will speed up this process, thus indicating that a small $\omega = \epsilon$ may satisfy Eq. (B2). In addition, according to Fig. 2, when ϕ is smaller than $\pi/4$, the length of the vector tends to decrease exponentially, and after it passes $\pi/4$ the length starts to increase exponentially. Therefore, the corresponding eigenstate is sharply localized at both edges. Except for this particular ϵ, we may expect that a vector with a slightly larger ω may pass two more quadrants to reach the negative y axis such that it can be another quasienergy of the system. But this is not true because the vector cannot go from the positive y axis to the negative x axis. Hence, this small quasienergy ϵ is well separated from other quasienergies. Until a quasienergy ω becomes large enough to cross the second quadrant (i.e., from the positive y axis to the negative x axis), no other ω can satisfy Eq. (B2).

APPENDIX C: OTHER SPECIAL QUASIENERGIES IN THE DISORDERED QW

Obuse *et al.* [20] numerically showed that $\omega = \pm\pi/2$ can be also special quasienergy values with singular DOS, which hence indicate the presence of ODD in disordered QW. Here we use the method developed in Sec. III to discuss these special quasienergy values.

We start with Eqs. (11) and (14) in Sec. II A. Without loss of generality, we choose $\omega = \pi/2$. Then the chain relation analogous to Eq. (15) will be

$$c_N \begin{pmatrix} -\sin\theta_0 \\ i \end{pmatrix} = \prod_{n=1}^{N} T_n \cdot c_0 \begin{pmatrix} i \\ \sin\theta_{N+1} \end{pmatrix} \quad \text{with} \quad T_n = i\sigma_z \sec\theta_n - \sigma_x \tan\theta_n. \tag{C1}$$

Define

$$P_m \equiv T_{2m} \cdot T_{2m-1}, \tag{C2}$$

so

$$P_m = (\tan\theta_{2m}\tan\theta_{2m-1} - \sec\theta_{2m}\sec\theta_{2m-1}) \cdot \boldsymbol{I} + (\sec\theta_{2m}\tan\theta_{2m-1} - \tan\theta_{2m}\sec\theta_{2m-1}) \cdot \sigma_y. \tag{C3}$$

Expressing P_m in the basis of σ_y, we have

$$P_m = \begin{pmatrix} -\cot\vartheta_{2m}\tan\vartheta_{2m-1} & 0 \\ 0 & -\tan\vartheta_{2m}\cot\vartheta_{2m-1} \end{pmatrix}, \tag{C4}$$

where $\vartheta_j = \frac{\pi}{4} - \frac{\theta_j}{2}$. So in the σ_y basis for even N,

$$\prod_{n=1}^{N} T_n = \begin{pmatrix} \lambda_+ & 0 \\ 0 & \lambda_- \end{pmatrix} \tag{C5}$$

with

$$\lambda_+ = \lambda_-^{-1} = (-1)^{\frac{N}{2}} \cot\vartheta_N \tan\vartheta_{N-1} \cdots \cot\vartheta_2 \tan\vartheta_1. \tag{C6}$$

Returning to the σ_z basis, we have

$$\prod_{n=1}^{N} T_n = \frac{1}{2}[(\lambda_+ + \lambda_-) \cdot \boldsymbol{I} + (\lambda_+ - \lambda_-) \cdot \sigma_y]. \tag{C7}$$

We substitute Eq. (C7) into Eq. (C1) and find that the boundary conditions $\theta_0 = \theta_{N+1} = \pm\pi/2$ will make Eq. (C1) hold, while $\theta_0 = \pi/2$, $\theta_{N+1} = -\pi/2$ or $\theta_0 = -\pi/2$, $\theta_{N+1} = \pi/2$ cannot. This conclusion is independent of the actual values of θ_n ($n = 1,2,\ldots,N$), so whether $\omega = \pi/2$ is the quasienergy of the system is determined by the boundary conditions, as well as the parity of the number of system sites.

In our setup, $N+2$ is the total number of sites in the disordered QW chain (See Fig. 1). Each bulk site corresponds to one transfer matrix, and totally N transfer matrices are involved in the calculation. When N is odd, one transfer matrix will be left if we pair those transfer matrices according to Eq. (C2). This leads to

$$\prod_{n=1}^{N} T_n = \frac{1}{2}(i\sigma_z \sec\theta_N - \sigma_x \tan\theta_N) \cdot [(\lambda'_+ + \lambda'_-) \cdot \boldsymbol{I} + (\lambda'_+ - \lambda'_-) \cdot \sigma_y], \tag{C8}$$

where λ'_+ and λ'_- are obtained from Eq. (C6) by substituting N with $N-1$. Different from the case of even N, the additional σ_x and σ_z flip the eigenspinors of σ_y, resulting in the opposite conclusions. In particular, boundary conditions $\theta_0 = \pi/2$, $\theta_{N+1} = -\pi/2$ or $\theta_0 = -\pi/2$, $\theta_{N+1} = \pi/2$ will give rise to $\omega = \pi/2$, while $\theta_0 = \theta_{N+1} = \pm\pi/2$ cannot.

We summarize the results in Table I. Those states with exactly quasienergy $\pm\pi/2$ are delocalized. For example, in the case of even N and $\theta_0 = \theta_{N+1} = -\pi/2$, we substitute Eq. (C7) into Eq. (C1) and get

$$c_N \begin{pmatrix} 1 \\ i \end{pmatrix} = i c_0 \lambda_+ \begin{pmatrix} 1 \\ i \end{pmatrix}. \tag{C9}$$

Therefore, the spinors at two boundaries are the eigenspinor of σ_y, and they are connected by λ_+ in Eq. (C6). In general $\lambda_+ \approx 1$ because $\cot\vartheta_j$ and $\tan\vartheta_k$ ($j,k \in [1,N]$ are arbitrary indices) will approximately cancel each other given that $\theta_{j\setminus k}$ are drawn randomly from a given distribution. This resembles the 0 mode in Sec. II B. Note that the delocalized 0mode requires θ_n to be drawn from a distribution symmetric with respect to $\theta = 0$ (we choose $\theta_n \in [-\Delta,\Delta]$ in our study), whereas the delocalized $\pm\pi/2$ states do not have this constraint. However, the advantage of a delocalized state at $\omega = 0$ is that it can be obtained from localized $\omega = 0$ state through an adiabatic protocol (See Sec. IV). By contrast, the $\omega = \pm\pi/2$ states cannot be obtained in this manner. The reason is simple. States with $\omega = \pm\pi/2$ are delocalized regardless of $\overline{\theta}$, the mean value of θ_n; whereas a delocalized $\omega = 0$ state requires $\overline{\theta} \approx 0$.

TABLE I. The existence (Y) or nonexistence (N) of $\pm\frac{\pi}{2}$ modes under different boundary conditions. In the bulk, values of θ_n ($1 \leqslant n \leqslant N$) are assumed not to satisfy $\pi/4 - \theta_n/2 = j \cdot \pi/2$ (j is an integer).

Boundary condition	$\omega = \pm\frac{\pi}{2}$, N even	$\omega = \pm\frac{\pi}{2}$, N odd
$\theta_0 = \frac{\pi}{2} = \theta_{N+1}$	Y	N
$\theta_0 = -\frac{\pi}{2}$, $\theta_{N+1} = \frac{\pi}{2}$	N	Y
$\theta_0 = \frac{\pi}{2}$, $\theta_{N+1} = -\frac{\pi}{2}$	N	Y
$\theta_0 = -\frac{\pi}{2} = \theta_{N+1}$	Y	N

[1] Y. Aharonov, L. Davidovich, and N. Zagury, Phys. Rev. A **48**, 1687 (1993).
[2] J. Kempe, Contemp. Phys. **44**, 307 (2003).
[3] E. Farhi and S. Gutmann, Phys. Rev. A **58**, 915 (1998).
[4] Y. Shikano, J. Comput. Theor. Nanosci. **10**, 1558 (2013).
[5] T. Kitagawa, M. S. Rudner, E. Berg, and E. Demler, Phys. Rev. A **82**, 033429 (2010).
[6] D. Y. H. Ho and J. Gong, Phys. Rev. Lett. **109**, 010601 (2012).
[7] B. Do, M. L. Stohler, S. Balasubramanian, D. S. Elliott, C. Eash, E. Fischbach, M. A. Fischbach, A. Mills, and B. Zwickl, J. Opt. Soc. Am. B **22**, 499 (2005).
[8] C. A. Ryan, M. Laforest, J. C. Boileau, and R. Laflamme, Phys. Rev. A **72**, 062317 (2005).
[9] H. Schmitz, R. Matjeschk, C. Schneider, J. Glueckert, M. Enderlein, T. Huber, and T. Schaetz, Phys. Rev. Lett. **103**, 090504 (2009).
[10] F. Zähringer, G. Kirchmair, R. Gerritsma, E. Solano, R. Blatt, and C. F. Roos, Phys. Rev. Lett. **104**, 100503 (2010).
[11] M. Karski, L. Förster, J.-M. Choi, A. Steffen, W. Alt, D. Meschede, and A. Widera, Science **325**, 174 (2009).
[12] H. B. Perets, Y. Lahini, F. Pozzi, M. Sorel, R. Morandotti, and Y. Silberberg, Phys. Rev. Lett. **100**, 170506 (2008).

[13] A. Peruzzo, M. Lobino, J. C. Matthews, N. Matsuda, A. Politi, K. Poulios, X.-Q. Zhou, Y. Lahini, N. Ismail, K. Wörhoff *et al.*, Science **329**, 1500 (2010).

[14] J. O. Owens, M. A. Broome, D. N. Biggerstaff, M. E. Goggin, A. Fedrizzi, T. Linjordet, M. Ams, G. D. Marshall, J. Twamley, M. J. Withford *et al.*, New J. Phys. **13**, 075003 (2011).

[15] L. Sansoni, F. Sciarrino, G. Vallone, P. Mataloni, A. Crespi, R. Ramponi, and R. Osellame, Phys. Rev. Lett. **108**, 010502 (2012).

[16] P. Zhang, X.-F. Ren, X.-B. Zou, B.-H. Liu, Y.-F. Huang, and G.-C. Guo, Phys. Rev. A **75**, 052310 (2007).

[17] M. A. Broome, A. Fedrizzi, B. P. Lanyon, I. Kassal, A. Aspuru-Guzik, and A. G. White, Phys. Rev. Lett. **104**, 153602 (2010).

[18] A. Schreiber, K. N. Cassemiro, V. Potoček, A. Gábris, P. J. Mosley, E. Andersson, I. Jex, and C. Silberhorn, Phys. Rev. Lett. **104**, 050502 (2010).

[19] F. Cardano, F. Massa, H. Qassim, E. Karimi, S. Slussarenko, D. Paparo, C. de Lisio, F. Sciarrino, E. Santamato, R. W. Boyd, and L. Marrucci, Science Advances **1**, e1500087 (2015).

[20] H. Obuse and N. Kawakami, Phys. Rev. B **84**, 195139 (2011).

[21] G. Theodorou and M. H. Cohen, Phys. Rev. B **13**, 4597 (1976).

[22] T. P. Eggarter and R. Riedinger, Phys. Rev. B **18**, 569 (1978).

[23] F. J. Dyson, Phys. Rev. **92**, 1331 (1953).

[24] M. R. Zirnbauer, Ann. Phys. (Berlin) **506**, 513 (1994).

[25] D.-H. Lee, Phys. Rev. B **50**, 10788 (1994).

[26] J. Kondev and J. Marston, Nucl. Phys. B **497**, 639 (1997).

[27] L. Balents and M. P. A. Fisher, Phys. Rev. B **56**, 12970 (1997).

[28] D. G. Shelton and A. M. Tsvelik, Phys. Rev. B **57**, 14242 (1998).

[29] R. G. Unanyan, J. Otterbach, M. Fleischhauer, J. Ruseckas, V. Kudriašov, and G. Juzeliūnas, Phys. Rev. Lett. **105**, 173603 (2010).

[30] M. J. Edmonds, J. Otterbach, R. G. Unanyan, M. Fleischhauer, M. Titov, and P. Öhberg, New J. Phys. **14**, 073056 (2012).

[31] M. Steiner, M. Fabrizio, and A. O. Gogolin, Phys. Rev. B **57**, 8290 (1998).

[32] L. Fleishman and D. C. Licciardello, J. Phys. C: Solid State Phys. **10**, L125 (1977).

[33] C. M. Soukoulis and E. N. Economou, Phys. Rev. B **24**, 5698 (1981).

[34] P. Markoš, Z. Phys. B: Condens. Matter **73**, 17 (1988).

[35] A. Bovier, J. Stat. Phys. **56**, 645 (1989).

[36] E. Lieb, T. Schultz, and D. Mattis, Ann Phys. (N.Y.) **16**, 407 (1961).

[37] E. R. Smith, J. Phys. C: Solid State Phys. **3**, 1419 (1970).

[38] A. W. W. Ludwig, M. P. A. Fisher, R. Shankar, and G. Grinstein, Phys. Rev. B **50**, 7526 (1994).

[39] P. W. Brouwer, E. Racine, A. Furusaki, Y. Hatsugai, Y. Morita, and C. Mudry, Phys. Rev. B **66**, 014204 (2002).

[40] F. A. de Moura and M. L. Lyra, Physica A: Statistical Mechanics and its Applications **266**, 465 (1999).

[41] H. Cheraghchi, S. M. Fazeli, and K. Esfarjani, Phys. Rev. B **72**, 174207 (2005).

[42] C. Zhou and R. N. Bhatt, Phys. Rev. B **68**, 045101 (2003).

[43] J. M. Zeuner, M. C. Rechtsman, S. Nolte, and A. Szameit, arXiv:1304.6911.

[44] M. Hase, I. Terasaki, Y. Sasago, K. Uchinokura, and H. Obara, Phys. Rev. Lett. **71**, 4059 (1993).

[45] S. B. Oseroff, S.-W. Cheong, B. Aktas, M. F. Hundley, Z. Fisk, and L. W. Rupp, Jr., Phys. Rev. Lett. **74**, 1450 (1995).

[46] M. Hase, K. Uchinokura, R. J. Birgeneau, K. Hirota, and G. Shirane, J. Phys. Soc. Jpn. **65**, 1392 (1996).

[47] T. Masuda, A. Fujioka, Y. Uchiyama, I. Tsukada, and K. Uchinokura, Phys. Rev. Lett. **80**, 4566 (1998).

[48] Y. J. Wang, V. Kiryukhin, R. J. Birgeneau, T. Masuda, I. Tsukada, and K. Uchinokura, Phys. Rev. Lett. **83**, 1676 (1999).

[49] H. Nakao, M. Nishi, Y. Fujii, T. Masuda, I. Tsukada, K. Uchinokura, K. Hirota, and G. Shirane, J. Phys. Chem. Solids **60**, 1117 (1999).

[50] R. Keil, J. M. Zeuner, F. Dreisow, M. Heinrich, A. Tünnermann, S. Nolte, and A. Szameit, Nat. Commun. **4**, 1368 (2013).

[51] T. Kitagawa, Quantum Inf. Process. **11**, 1107 (2012).

[52] J. K. Asbóth, Phys. Rev. B **86**, 195414 (2012).

[53] P. Markoš and C. M. Soukoulis, in *Wave Propagation: From Electrons to Photonic Crystals and Left-Handed Materials* (Princeton University Press, Princeton and Oxford, 2008), Chaps. 1–4.

[54] C. A. Müller and D. Delande, in *Ultracold Gases and Quantum Information*, Lecture Notes of the Les Houches Summer School, Vol. 91, edited by C. Miniatura, L.-C. Kwek, M. Ducloy, B. Grémaud, B.-G. Englert, L. Cugliandolo, A. Ekert, and K. K. Phua (Oxford University Press, Oxford, 2011), Chap. 9.

[55] H. Schmidt, Phys. Rev. **105**, 425 (1957).

[56] A. Dranov, J. Kellendonk, and R. Seiler, J. Math. Phys. **39**, 1340 (1998).

[57] A. Tanaka, J. Phys. Soc. Japan **80**, 125002 (2011).

[58] H. Wang, L. Zhou, and J. Gong, Phys. Rev. B **91**, 085420 (2015).